Superradiant and Subradiant Cavity Scattering by Atom Arrays

Zhenjie Yan,[1,2] Jacquelyn Ho,[1,2] Yue-Hui Lu,[1,2] Stuart J. Masson,[3] Ana Asenjo-Garcia,[3] and Dan M. Stamper-Kurn[1,2,4,*]

[1]Department of Physics, University of California, Berkeley, California 94720, USA
[2]Challenge Institute for Quantum Computation, University of California, Berkeley, California 94720, USA
[3]Department of Physics, Columbia University, New York, New York 10027, USA
[4]Materials Sciences Division, Lawrence Berkeley National Laboratory, Berkeley, California 94720, USA

(Received 27 July 2023; accepted 2 November 2023; published 21 December 2023)

We realize collective enhancement and suppression of light scattered by an array of tweezer-trapped ^{87}Rb atoms positioned within a strongly coupled Fabry-Pérot optical cavity. We illuminate the array with light directed transverse to the cavity axis, in the low saturation regime, and detect photons scattered into the cavity. For an array with integer-optical-wavelength spacing each atom scatters light into the cavity with nearly identical scattering amplitude, leading to an observed N^2 scaling of cavity photon number as the atom number increases stepwise from $N = 1$ to $N = 8$. By contrast, for an array with half-integer-wavelength spacing, destructive interference of scattering amplitudes yields a nonmonotonic, subradiant cavity intensity versus N. By analyzing the polarization of light emitted from the cavity, we find that Rayleigh scattering can be collectively enhanced or suppressed with respect to Raman scattering. We observe also that atom-induced shifts and broadenings of the cavity resonance are precisely tuned by varying the atom number and positions. Altogether, tweezer arrays provide exquisite control of atomic cavity QED spanning from the single- to the many-body regime.

DOI: 10.1103/PhysRevLett.131.253603

As highlighted by Dicke's seminal work on super- and subradiance [1], the interaction of multiple emitters with a quantum mode of light differs from that of the emitters individually. Collective "superradiant" (or "bright") states, resulting from constructive interference, give rise to an enhanced emission rate per excitation, which grows with the number of emitters. Conversely, "subradiant" (or "dark") states arise from destructive interference, leading to a suppression or complete cancellation of photon emission.

In the case of extended samples, with emitters distributed over distances longer than the emitted optical wavelength, the observation and control of super- and subradiance depends critically on the exact spatial distribution of the emitters. For example, the precise structure of mesoscopic samples [2–4] or periodic emitter arrays [5–7] controls whether their collective emission is enhanced or suppressed, or directed into single or multiple optical modes.

In cavity quantum electrodynamics (QED), in which each of multiple emitters couples strongly to a single-mode cavity field, the properties of (and the access to) the bright and dark manifolds depend strongly on the spatial positions of emitters within the cavity. Already for single emitters, controlling the position of atoms in a cavity advanced the field of cavity QED [8–11]. Basic effects of few-body cavity QED have been illustrated by the controlled placement of two atoms [12,13] or ions [14,15] within resonant cavities. Experiments on superconducting quantum circuits have extended studies of collective emission into microwave cavities and waveguides to as many as 10 qubits [16–20].

In this Letter, we employ deterministically loaded atom tweezer arrays [21,22], a powerful new platform for quantum simulation [23], metrology [24,25], and information processing [26], to advance atomic cavity QED from the few- to the many-body regime while preserving precise control over the cavity interaction of each individual atom.

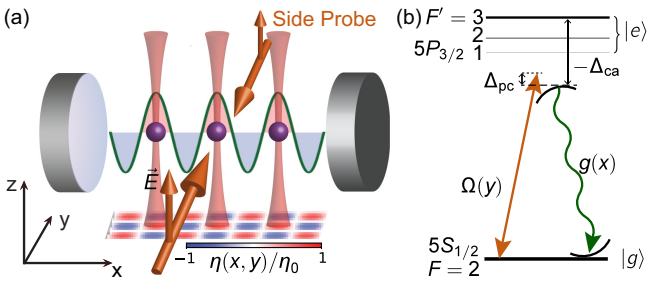

FIG. 1. Schematic of the experimental setup. (a) Atoms are driven by a pair of counter propagating side probe beams. The two-photon scattering amplitude $\eta(x, y)$ from the probe beam into the cavity, by an atom located at (x, y), exhibits a two-dimensional checkerboard pattern. (b) The probe light (orange) and the cavity photons (green) couple the $F = 2$ hyperfine states of the $5S_{1/2}$ atomic ground state with the $5P_{3/2}$ excited states. Three hyperfine manifolds $F' = 3$, 2, 1 of the excited states contribute to the probe-cavity scattering.

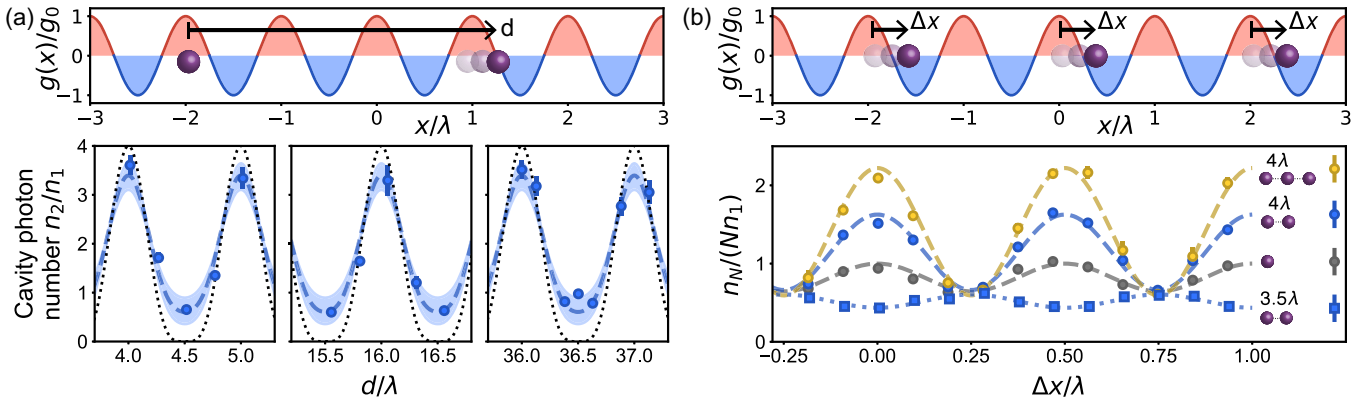

FIG. 2. (a) Cavity scattering by a two-atom array. One atom is placed at a cavity antinode, and scatters with steady-state cavity photon number n_1 on its own. Adding a second atom, at a distance d from the first, changes the cavity photon number to n_2. Expected ratios n_2/n_1 for perfectly localized atoms (dotted black line) and atoms with $\sigma = 100(14)$ nm position fluctuations (dashed blue line, uncertainty in σ indicated by shaded area). (b) Normalized cavity photon number $n_N/(Nn_1)$ generated by N-atom arrays with fixed spacing, displaced by Δx from a cavity antinode. The array has $N = 1$ (gray), 2 (blue), 3 (yellow) atoms, and a spacing of 4λ (circles) or 3.5λ (squares). The dashed and dotted lines are cosinusoidal fits with a period of $\lambda/2$. All data are taken with $\Delta_{pc} = 0$.

With such a tweezer array, we place a fixed number of ^{87}Rb atoms at fully controlled positions along the axis of a strongly coupled Fabry-Pérot optical resonator [27,28] [Fig. 1(a)]. This method improves upon the incomplete control of atom number, position, and motion in previous approaches used in trapped-atom and -ion cavity QED experiments [29,30]. By driving this emitter array with light propagating transverse to the cavity axis while monitoring the cavity emission, we prepare both super- and subradiant (single-excitation) states. We characterize these states via the number of photons present in the cavity, which scales as N^2 for superradiant states and sublinearly for subradiant ones.

We employ an in-vacuum near-concentric Fabry-Pérot optical cavity with a TEM_{00} mode whose frequency (ω_c) lies near the transition frequency (ω_a) of the ^{87}Rb $F = 2 \rightarrow F' = 3$ D_2 transition (wavelength $\lambda = 780$ nm) [31,32]. Near the cavity center, the coupling amplitude of a single ^{87}Rb atom to this cavity mode varies as $g(x) = g_0 \cos kx$; here, $g_0 = 2\pi \times 3.1$ MHz (on the cycling transition) and $k = 2\pi/\lambda$. Given the atomic and cavity resonance half-linewidths of $\gamma = 2\pi \times 3.0$ MHz and $\kappa = 2\pi \times 0.53$ MHz, respectively, the cavity achieves the strong coupling condition with single-atom cooperativity $C = g_0^2/(2\kappa\gamma) = 3.0$ [33].

A one-dimensional array of optical tweezers is formed by laser beams with a wavelength of 808 nm sent transversely to the cavity through a high numerical-aperture imaging system. Precooled and optically trapped ^{87}Rb atoms are loaded into as many as 16 tweezers, detected through fluorescence imaging, and then sorted into regularly spaced arrays of $N = 1$ to 8 atoms [34]. The total length of these arrays is much smaller than the $\sim$1 mm cavity Rayleigh range. The array is aligned to place atoms at the radial center of the cavity. Piezocontrolled mirrors and an acousto-optical deflector are used to position the array with nanometer-scale precision along the cavity axis.

Our experiments focus on the response of this atom array when it is driven optically. For this, we illuminate the array with a transverse standing wave of monochromatic probe light, see Fig. 1(a). The probe is linearly polarized along the z axis (chosen as our quantization axis), perpendicular to the cavity, and drives each atom with a spatially dependent Rabi frequency $\Omega(y) = \Omega_0 \cos ky$. The standing-wave configuration balances photon recoil momentum, allows for positional calibration along the y axis, and reduces incoherence in photon emission caused by atomic thermal motion [34]. We employ a weak probe amplitude to ensure that the probability of having more than one atom excited simultaneously is negligible. All tweezer traps are centered at $y = 0$. The probe frequency ω_p operates at a small detuning $\Delta_{pc} = \omega_p - \omega_c$ from the cavity resonance [Fig. 1(b)]. Prior to probe illumination, the tweezer-trapped atoms are polarization-gradient cooled and prepared in the $F = 2$ ground hyperfine manifold, without control of their Zeeman state. Probe light scattered by the array into the cavity, and thence through one mirror of our one-sided cavity, is detected by a single-photon counting module.

To demonstrate the strong sensitivity of collective cavity scattering on the exact positioning of the scatterers, we first examine an array of just two atoms. As illustrated in Fig. 2(a), we first position one atom at an antinode of the cavity field. With the cavity at a large detuning $\Delta_{ca} = \omega_c - \omega_a = -2\pi \times 507$ MHz—a specific "magic" value chosen to suppress fluctuations from internal-state dynamics, as described below—we denote the steady-state cavity photon number generated by this single atom as n_1. We then add a second atom at a variable distance d from the first, and record the cavity photon number produced by the atom pair as n_2. At integer-wavelength separation

($d = m\lambda$ with m an integer), we observe superradiant light scattering, where the total cavity emission rate is greater than that of two individual atoms ($n_2 > 2n_1$). At half-integer-wavelength separation [$d = (m + 1/2)\lambda$], we observe subradiant light scattering ($n_2 < 2n_1$).

To account for the observed behavior, let us consider that each atom i, positioned at location (x_i, y_i), serves as a source for light in the cavity, with elastic scattering amplitude $\eta(x_i, y_i) = g(x_i)\Omega(y_i)/2\Delta_{ca} \equiv \eta_0 \cos kx_i \cos ky_i$, which we obtain by treating the atom as a two-level emitter and adiabatically eliminating its excited state. The scattering amplitudes from all atoms add coherently. The steady-state cavity photon number scattered by N atoms is then $n_N = |\bar{a}|^2$, where the expectation value of the cavity-field amplitude is given, following a semiclassical treatment [34,36,37] in the dispersive coupling regime $|\Delta_{ca}| \gg \{\Omega_0, g_0, \gamma\}$, as

$$\bar{a} = \frac{\sum_i \eta(x_i, y_i)}{[\Delta_{pc} - \sum_i g^2(x_i)/\Delta_{ca}] + i[\kappa + \sum_i \gamma g^2(x_i)/\Delta_{ca}^2]}. \quad (1)$$

Here, we have accounted for the atom-induced dispersive shift $\sum_i g^2(x_i)/\Delta_{ca}$ and absorptive broadening $\sum_i \gamma g^2(x_i)/\Delta_{ca}^2$ of the cavity resonance.

At large $|\Delta_{ca}|$, where we can neglect atom-induced modifications of the cavity resonance, and with $\Delta_{pc} = 0$, the cavity photon number varies simply as $n_N = |\sum_i \eta(x_i, y_i)|^2/\kappa^2$. For two atoms, with the first situated exactly at the antinode and the second at an exact axial distance d, one then expects $n_2/n_1 = [1 + \cos kd]^2$, with limiting values $n_2/n_1 = 4$ from constructive interference at integer-wavelength separation, and $n_2/n_1 = 0$ from destructive interference at half-integer-wavelength separation. In our experiment, uncorrelated fluctuations in η, deriving from thermal position fluctuations of the two atoms within their tweezer traps, constrain these limiting values to $n_2/n_1 = 2(1 \pm D)$, where the ratio $D = |\langle\eta\rangle|^2/\langle|\eta|^2\rangle$ is the Debye-Waller factor and $\langle\rangle$ denotes an average over the position distribution of a single trapped atom. The data in Fig. 2(a) are consistent with root mean square variations of $\sigma = 100(14)$ nm in both the x and y directions of motion, with σ determined independently by measuring light scattering from a single atom [34]. In future work, σ can be reduced further through bursts of dark-state cooling [38–40]. A strong contrast between constructive and destructive interference is retained even at large atomic separations—as far as $d \simeq 30$ μm.

The photon scattering rate also depends on the positions of the atoms with respect to the standing-wave cavity mode. We illustrate this dependence by measuring light scattering from atom arrays with fixed integer- or half-integer-wavelength spacing while translating these arrays altogether by Δx from a cavity antinode [Fig. 2(b)]. Again, we observe either super- or subradiance when the array is aligned onto cavity antinodes. In contrast, when either type of array is aligned to cavity nodes, we observe scattering that scales linearly with N. Here, position fluctuations cause the scattering amplitude from each atom to vary between positive and negative values with equal probability, producing a cavity field with finite variance but zero average amplitude.

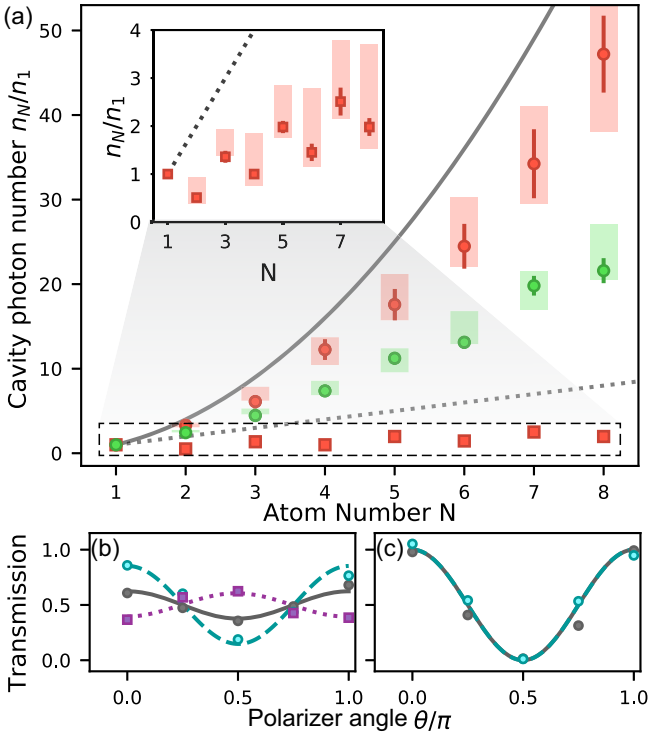

FIG. 3. (a) Normalized cavity photon number (n_N/n_1) for scattering by N-atom arrays with either integer- (circles, $d = 5.0\lambda$) or half-integer- (squares, $d = 5.5\lambda$) wavelength spacing, using cavity-atom detuning at either $\Delta_{ca} = -2\pi \times 507$ MHz (red) or $-2\pi \times 38$ MHz (green). Inset: close-up data from half-integer-wavelength arrays. The solid (dashed) black line corresponds to a quadratic N^2 (linear N) scaling. The red shaded area is calculated from Eqs. (2) and (3), while the green shaded area is the result of a Monte Carlo calculation assuming equal population among all m_F states [34]. (b),(c) Polarization analysis of cavity emission. Relative transmission through a linear polarizer at an angle θ with respect to the z axis at (b) $\Delta_{ca} = -2\pi \times 38$ MHz and (c) $\Delta_{ca} = -2\pi \times 507$ MHz. Shown for scattering by a single atom (gray circles), or $N = 8$ atoms at the constructive (cyan circles) or the destructive interference condition (purple squares). The corresponding curves show results of the Monte Carlo calculation.

The superradiant emission by atoms at the constructive interference condition is further enhanced by increasing the atom number [Fig. 3(a)]. At large $|\Delta_{ca}|$ and on cavity resonance, the number of cavity photons emitted by an N-atom array is predicted to be

$$n_N = [N(\langle|\eta|^2\rangle - |\langle\eta\rangle|^2) + N^2|\langle\eta\rangle|^2]/\kappa^2. \quad (2)$$

This expression consists of an incoherent part that scales linearly with N and that vanishes if atoms are fully

localized ($\sigma = 0$), and a coherent part that scales quadratically as N^2. Our measurements with N ranging from 1 to 8 match well with this prediction, clearly exhibiting superradiant scattering.

At the destructive interference condition, i.e., an atom array with half-integer-wavelength spacing, collective scattering is subradiant, falling below the linear scaling with N expected for an incoherent sample. Here, at similar probe and cavity settings, one expects the cavity photon number to vary as

$$n_N = \left[N(\langle|\eta^2|\rangle - |\langle\eta\rangle|^2) + \frac{1-(-1)^N}{2}|\langle\eta\rangle|^2\right]/\kappa^2. \quad (3)$$

While the incoherent scattering rate remains linear in N, the coherent photon scattering by pairs of atoms with opposite phase cancel out, resulting in a total coherent contribution equal to that of either zero emitters (even N) or a single emitter (odd N). The nonmonotonic behavior observed in our experiment emerges as the coherent scattering rate exceeds the incoherent one: $|\langle\eta\rangle|^2 > \langle|\eta^2|\rangle - |\langle\eta\rangle|^2$.

At smaller detuning $|\Delta_{ca}|$, collective light scattering is affected by two additional effects. First, coherent scattering is degraded by polarization and intensity fluctuations arising from internal state dynamics of the multilevel ^{87}Rb atom. In our setup, incoherent Raman scattering causes each atom's magnetic quantum number m_F to be distributed among all possible values. For small $\Delta_{ca} = -2\pi \times 38$ MHz, the amplitude η for emitting z-polarized light, arising primarily from the near-resonant $F = 2 \rightarrow F' = 3$ transition, varies strongly with m_F. This random variation further degrades the Debye-Waller factor, reducing the collective enhancement of light scattering as shown in Fig. 3(a).

Furthermore, at this detuning, atoms can scatter the z-polarized probe light into cavity modes of two orthogonal polarizations. Scattering into the z-polarized cavity mode, i.e., Rayleigh scattering, does not change the spin state of the ground-state atoms. The final spin state after Rayleigh scattering is independent of which atom scattered a photon. Thus, the Rayleigh scattering rate is determined by the interference of the scattering amplitudes from all atoms, allowing for enhancement or suppression. In contrast, scattering into the y-polarized cavity mode, i.e., Raman scattering, does change the spin state of the ground state. In our experiment, it is reasonable to assume the ground-state atoms are, at all times, in an incoherent mixture of spin states owing to imprecise initial state preparation and rapid state collapse caused by incoherent light scattering. Given that the final spin states produced by each atom Raman scattering a photon are orthogonal, and absent coherence among initial spin states, the Raman scattering rates in our experiment add incoherently. By operating in other regimes which allow for coherences among the ground states, collective Raman scattering can indeed be observed [41–44].

In support of this description, we examine separately the cavity emission of z- and y-polarized light [Fig. 3(b)]. At small detuning, and in comparison to the light polarization emitted by a single atom, the emission of z-polarized light (relative to y-polarized light) is enhanced by superradiant scattering at integer-wavelength atomic spacing and suppressed by subradiant scattering at half-integer-wavelength atomic spacing.

For much of our Letter, we avoid these internal-state and polarization effects by operating at the aforementioned "magic" detuning of $\Delta_{ca} = -2\pi \times 507$ MHz [34,45]. Here, when accounting for transitions to all three accessible excited hyperfine states ($F' = 1$, 2, and 3), the amplitude for scattering z-polarized light is nearly identical for all Zeeman states within the ground $F = 2$ manifold. Simultaneously, the rate for Raman scattering y-polarized light is nearly extinguished, as observed in the nearly pure z polarization of light emitted from the cavity [Fig. 3(c)]. The identification of such a "magic" detuning for nearly all alkali species [34,45], which allows light scattering by an alkali atom to resemble closely that of just a two-level atom, should be beneficial to other quantum optics experiments using alkali gases.

Additionally, at small detuning, we observe significant modifications of the cavity resonance by the atomic array within. As shown in Fig. 4(a), we record n_N for various arrays as a function of the detuning Δ_{pc} of the probe from the empty-cavity resonance. From the observed emission line shapes, we extract the atom-induced cavity resonance shift and also the total cavity linewidth. The measured spectral shifts and widths show a near-linear dependence on the atom number N [Figs. 4(c) and 4(d)], and agree well with a theoretical calculation accounting for both atomic position and m_F fluctuations [34]. Owing to the $g^2(x_i)$ dependence of the cavity dispersion and absorption terms, the atom-induced cavity modification is the same for atoms at both integer- and half-integer-wavelength spacing. Notably, these modifications are reduced for atom arrays centered on the cavity field nodes, and such spatial dependence is the foundation of optomechanical coupling between the atomic motion and the cavity field [46,47]. By comparison, the atom-induced cavity modifications are all negligible for large $|\Delta_{ca}|$.

While the current work explores only the bottom of the Dicke ladder, where only one atom is excited, our platform enables study of many-excitation super- or subradiance [1,48], up to full or zero state inversion, respectively, with unprecedented control. The interplay between atomic quantum states, collective atom-cavity interaction, and optical emission properties can be fully explored [49]. Our setup would provide insight into key features of many-body decay in the presence of multiple decay channels (due to the multimode nature of the cavity), such as the scaling with atom number of the peak intensity and the time of peak

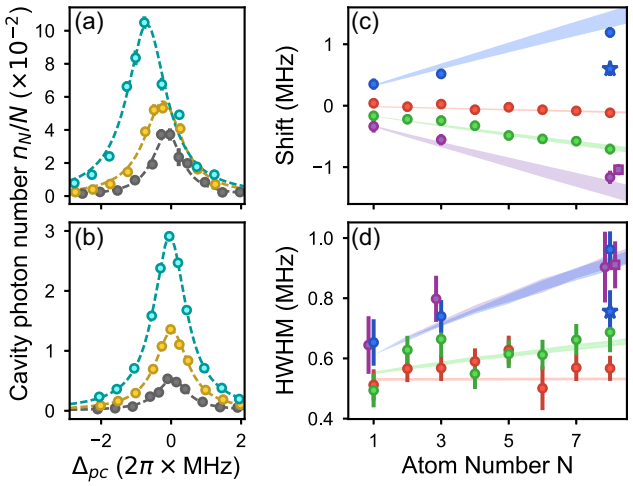

FIG. 4. Cavity spectra measured with arrays of $N = 1$ (black), 3 (yellow), and 8 (cyan) at (a) $\Delta_{ca} = -2\pi \times 38$ MHz and (b) $-2\pi \times 507$ MHz. All atoms are aligned with cavity antinodes of the same phase. Lorentzian fits (dashed lines) are used to determine the peak positions and linewidths. The cavity resonance (c) shifts and (d) half widths at half maximum (HWHM) as a function of atom number, measured with all atoms aligned with cavity antinodes of the same phase (circles), at detunings of $\Delta_{ca} = -2\pi \times 507$ MHz (red), $-2\pi \times 38$ MHz (green), $-2\pi \times 19$ MHz (purple), and $2\pi \times 19$ MHz (blue). The corresponding shaded areas are predictions from a Monte Carlo calculation [34]. Results are also shown for an array with half-integer-wavelength spacing at the cavity antinodes (squares), and an array with integer-wavelength spacing at the cavity nodes (stars). For clarity, some symbols in (c) and (d) are slightly offset in N.

emission, as well as large shot-to-shot fluctuations [50–52] in the light polarization due to self-reinforcing feedback.

Our realization of a well-controlled many-body cavity QED system, compatible with single-atom control, offers a wide range of potential quantum applications. When single-photon cavity emission is subradiantly suppressed, multi-photon emission becomes the dominant process, leading to a nonlinear photon source [13,53]. Encoding quantum information in a symmetrically excited W state or related states [54] can superradiantly speed up information exchange between matter and itinerant photons. This accelerates quantum communications and reduces the infidelity accumulated over the interaction time [14,55]. The possibility of switching between super- and subradiant states, through either phase rotation on individual atoms or moving the tweezers, allows on-demand multiphoton storage and emission [56].

Finally, coherent long-range photon-mediated momentum [30,57,58] or spin [59–63] exchanges between individual atoms can be facilitated through subsequent absorption of the cavity photons by the atoms and can be used for quantum simulation on the Dicke model [64], entanglement generation [65], or realization of quantum solvers [66]. Notably, atom arrays that combine long-range photon-mediated interactions with short-range Rydberg interactions could benefit from the advantages of both types of interactions with distinct ranges, connectivity, and timescales [67–69].

We acknowledge support from the AFOSR (Grant No. FA9550-1910328 and Young Investigator Prize Grant No. 21RT0751), from ARO through the MURI program (Grant No. W911NF-20-1-0136), from DARPA (Grant No. W911NF2010090), from the NSF (QLCI program through Grant No. OMA-2016245, and CAREER Award No. 2047380), and from the David and Lucile Packard Foundation. J. H. acknowledges support from the National Defense Science and Engineering Graduate (NDSEG) fellowship. We thank Erhan Saglamyurek for helpful discussions. We also thank Jacopo De Santis, Florian Zacherl, and Nathan Song for their assistance in the lab.

*dmsk@berkeley.edu

[1] R. H. Dicke, Coherence in spontaneous radiation processes, Phys. Rev. **93**, 99 (1954).
[2] J. P. Clemens, L. Horvath, B. C. Sanders, and H. J. Carmichael, Collective spontaneous emission from a line of atoms, Phys. Rev. A **68**, 023809 (2003).
[3] S. J. Masson, I. Ferrier-Barbut, L. A. Orozco, A. Browaeys, and A. Asenjo-Garcia, Many-body signatures of collective decay in atomic chains, Phys. Rev. Lett. **125**, 263601 (2020).
[4] M. O. Scully, E. S. Fry, C. H. R. Ooi, and K. Wódkiewicz, Directed spontaneous emission from an extended ensemble of N atoms: Timing is everything, Phys. Rev. Lett. **96**, 010501 (2006).
[5] S. J. Masson and A. Asenjo-Garcia, Universality of Dicke superradiance in arrays of quantum emitters, Nat. Commun. **13**, 2285 (2022).
[6] H. Tamura, H. Nguyen, P. R. Berman, and A. Kuzmich, Phase matching in lower dimensions, Phys. Rev. Lett. **125**, 163601 (2020).
[7] J. Rui, D. Wei, A. Rubio-Abadal, S. Hollerith, J. Zeiher, D. M. Stamper-Kurn, C. Gross, and I. Bloch, A subradiant optical mirror formed by a single structured atomic layer, Nature (London) **583**, 369 (2020).
[8] G. R. Guthöhrlein, M. Keller, K. Hayasaka, W. Lange, and H. Walther, A single ion as a nanoscopic probe of an optical field, Nature (London) **414**, 49 (2001).
[9] S. Nußmann, M. Hijlkema, B. Weber, F. Rohde, G. Rempe, and A. Kuhn, Submicron positioning of single atoms in a microcavity, Phys. Rev. Lett. **95**, 173602 (2005).
[10] A. Reiserer, C. Nölleke, S. Ritter, and G. Rempe, Ground-state cooling of a single atom at the center of an optical cavity, Phys. Rev. Lett. **110**, 223003 (2013).
[11] J. D. Thompson, T. G. Tiecke, N. P. de Leon, J. Feist, A. V. Akimov, M. Gullans, A. S. Zibrov, V. Vuletić, and M. D. Lukin, Coupling a single trapped atom to a nanoscale optical cavity, Science **340**, 1202 (2013).

[12] R. Reimann, W. Alt, T. Kampschulte, T. Macha, L. Ratschbacher, N. Thau, S. Yoon, and D. Meschede, Cavity-modified collective Rayleigh scattering of two atoms, Phys. Rev. Lett. **114**, 023601 (2015).
[13] A. Neuzner, M. Körber, O. Morin, S. Ritter, and G. Rempe, Interference and dynamics of light from a distance-controlled atom pair in an optical cavity, Nat. Photonics **10**, 303 (2016).
[14] B. Casabone, K. Friebe, B. Brandstätter, K. Schüppert, R. Blatt, and T. E. Northup, Enhanced quantum interface with collective ion-cavity coupling, Phys. Rev. Lett. **114**, 023602 (2015).
[15] S. Begley, M. Vogt, G. K. Gulati, H. Takahashi, and M. Keller, Optimized multi-ion cavity coupling, Phys. Rev. Lett. **116**, 223001 (2016).
[16] J. Majer, J. M. Chow, J. M. Gambetta, J. Koch, B. R. Johnson, J. A. Schreier, L. Frunzio, D. I. Schuster, A. A. Houck, A. Wallraff, A. Blais, M. H. Devoret, S. M. Girvin, and R. J. Schoelkopf, Coupling superconducting qubits via a cavity bus, Nature (London) **449**, 443 (2007).
[17] A. F. van Loo, A. Fedorov, K. Lalumière, B. C. Sanders, A. Blais, and A. Wallraff, Photon-mediated interactions between distant artificial atoms, Science **342**, 1494 (2013).
[18] M. Mirhosseini, E. Kim, X. Zhang, A. Sipahigil, P. B. Dieterle, A. J. Keller, A. Asenjo-Garcia, D. E. Chang, and O. Painter, Cavity quantum electrodynamics with atom-like mirrors, Nature (London) **569**, 692 (2019).
[19] B. Kannan, M. J. Ruckriegel, D. L. Campbell, A. Frisk Kockum, J. Braumüller, D. K. Kim, M. Kjaergaard, P. Krantz, A. Melville, B. M. Niedzielski, A. Vepsäläinen, R. Winik, J. L. Yoder, F. Nori, T. P. Orlando, S. Gustavsson, and W. D. Oliver, Waveguide quantum electrodynamics with superconducting artificial giant atoms, Nature (London) **583**, 775 (2020).
[20] Z. Wang, H. Li, W. Feng, X. Song, C. Song, W. Liu, Q. Guo, X. Zhang, H. Dong, D. Zheng, H. Wang, and D.-W. Wang, Controllable switching between superradiant and subradiant states in a 10-qubit superconducting circuit, Phys. Rev. Lett. **124**, 013601 (2020).
[21] M. Endres, H. Bernien, A. Keesling, H. Levine, E. R. Anschuetz, A. Krajenbrink, C. Senko, V. Vuletic, M. Greiner, and M. D. Lukin, Atom-by-atom assembly of defect-free one-dimensional cold atom arrays, Science **354**, 1024 (2016).
[22] D. Barredo, S. D. Léséleuc, V. Lienhard, T. Lahaye, and A. Browaeys, Atomic arrays, Science **354**, 1021 (2016).
[23] A. Browaeys and T. Lahaye, Many-body physics with individually controlled Rydberg atoms, Nat. Phys. **16**, 132 (2020).
[24] I. S. Madjarov, A. Cooper, A. L. Shaw, J. P. Covey, V. Schkolnik, T. H. Yoon, J. R. Williams, and M. Endres, An atomic-array optical clock with single-atom readout, Phys. Rev. X **9**, 041052 (2019).
[25] A. W. Young, W. J. Eckner, W. R. Milner, D. Kedar, M. A. Norcia, E. Oelker, N. Schine, J. Ye, and A. M. Kaufman, Half-minute-scale atomic coherence and high relative stability in a tweezer clock, Nature (London) **588**, 408 (2020).
[26] A. M. Kaufman and K. K. Ni, Quantum science with optical tweezer arrays of ultracold atoms and molecules, Nat. Phys. **17**, 1324 (2021).
[27] Y. Liu, Z. Wang, P. Yang, Q. Wang, Q. Fan, S. Guan, G. Li, P. Zhang, and T. Zhang, Realization of strong coupling between deterministic single-atom arrays and a high-finesse miniature optical cavity, Phys. Rev. Lett. **130**, 173601 (2023).
[28] An earlier experiment, reported in Ref. [27], showcased the strong collective coupling between a cavity and an array of atoms within a combined optical potential of a tweezer array and an optical lattice. However, control over the phase and amplitude of the atom-cavity interaction was not demonstrated in that work.
[29] A. Reiserer and G. Rempe, Cavity-based quantum networks with single atoms and optical photons, Rev. Mod. Phys. **87**, 1379 (2015).
[30] F. Mivehvar, F. Piazza, T. Donner, and H. Ritsch, Cavity QED with quantum gases: New paradigms in many-body physics, Adv. Phys. **70**, 1 (2021).
[31] E. Deist, J. A. Gerber, Y.-H. Lu, J. Zeiher, and D. M. Stamper-Kurn, Superresolution microscopy of optical fields using tweezer-trapped single atoms, Phys. Rev. Lett. **128**, 083201 (2022).
[32] E. Deist, Y.-H. Lu, J. Ho, M. K. Pasha, J. Zeiher, Z. Yan, and D. M. Stamper-Kurn, Mid-circuit cavity measurement in a neutral atom array, Phys. Rev. Lett. **129**, 203602 (2022).
[33] H. J. Kimble, Strong interactions of single atoms and photons in cavity QED, Phys. Scr. T **76**, 127 (1998).
[34] See Supplemental Material at http://link.aps.org/supplemental/10.1103/PhysRevLett.131.253603 for details on experimental methods and theories of collective cavity scattering, which includes Ref. [35].
[35] I. S. Madjarov, Entangling, controlling, and detecting individual strontium atoms in optical tweezer arrays, Ph.D. thesis, California Institute of Technology, 2021, 10.7907/d1em-dt34.
[36] P. Domokos and H. Ritsch, Collective cooling and self-organization of atoms in a cavity, Phys. Rev. Lett. **89**, 253003 (2002).
[37] H. Tanji-Suzuki, I. D. Leroux, M. H. Schleier-Smith, M. Cetina, A. T. Grier, J. Simon, and V. Vuletić, Interaction between atomic ensembles and optical resonators, Adv. At. Mol. Opt. Phys. **60**, 201 (2011).
[38] A. M. Kaufman, B. J. Lester, and C. A. Regal, Cooling a single atom in an optical tweezer to its quantum ground state, Phys. Rev. X **2**, 041014 (2012).
[39] J. Ang'ong'a, C. Huang, J. P. Covey, and B. Gadway, Gray molasses cooling of ^{39}K atoms in optical tweezers, Phys. Rev. Res. **4**, 013240 (2022).
[40] M. O. Brown, T. Thiele, C. Kiehl, T.-W. Hsu, and C. A. Regal, Gray-molasses optical-tweezer loading: Controlling collisions for scaling atom-array assembly, Phys. Rev. X **9**, 011057 (2019).
[41] J. G. Bohnet, Z. Chen, J. M. Weiner, D. Meiser, M. J. Holland, and J. K. Thompson, A steady-state superradiant laser with less than one intracavity photon, Nature (London) **484**, 78 (2012).
[42] Z. Zhiqiang, C. H. Lee, R. Kumar, K. J. Arnold, S. J. Masson, A. S. Parkins, and M. D. Barrett, Nonequilibrium phase transition in a spin-1 Dicke model, Optica **4**, 424 (2017).

[43] M. Landini, N. Dogra, K. Kroeger, L. Hruby, T. Donner, and T. Esslinger, Formation of a spin texture in a quantum gas coupled to a cavity, Phys. Rev. Lett. **120**, 223602 (2018).
[44] R. M. Kroeze, Y. Guo, V. D. Vaidya, J. Keeling, and B. L. Lev, Spinor self-ordering of a quantum gas in a cavity, Phys. Rev. Lett. **121**, 163601 (2018).
[45] S. J. Masson, Z. Yan, J. Ho, Y.-H. Lu, D. M. Stamper-Kurn, and A. Asenjo-Garcia, State-insensitive wavelengths for light shifts and photon scattering from Zeeman states, arXiv:2312.08370.
[46] K. Baumann, C. Guerlin, F. Brennecke, and T. Esslinger, Dicke quantum phase transition with a superfluid gas in an optical cavity, Nature (London) **464**, 1301 (2010).
[47] J. Kohler, J. A. Gerber, E. Dowd, and D. M. Stamper-Kurn, Negative-mass instability of the spin and motion of an atomic gas driven by optical cavity backaction, Phys. Rev. Lett. **120**, 013601 (2018).
[48] M. Gross and S. Haroche, Superradiance: An essay on the theory of collective spontaneous emission, Phys. Rep. **93**, 301 (1982).
[49] C. Hotter, L. Ostermann, and H. Ritsch, Cavity sub- and superradiance for transversely driven atomic ensembles, Phys. Rev. Res. **5**, 013056 (2023).
[50] J. P. Clemens, L. Horvath, B. C. Sanders, and H. J. Carmichael, Shot-to-shot fluctuations in the directed superradiant emission from extended atomic samples, J. Opt. B **6**, S736 (2004).
[51] A. Piñeiro Orioli, J. K. Thompson, and A. M. Rey, Emergent dark states from superradiant dynamics in multilevel atoms in a cavity, Phys. Rev. X **12**, 011054 (2022).
[52] S. Cardenas-Lopez, S. J. Masson, Z. Zager, and A. Asenjo-Garcia, Many-body superradiance and dynamical mirror symmetry breaking in waveguide QED, Phys. Rev. Lett. **131**, 033605 (2023).
[53] H. Habibian, S. Zippilli, and G. Morigi, Quantum light by atomic arrays in optical resonators, Phys. Rev. A **84**, 033829 (2011).
[54] A. Cabello, Bell's theorem with and without inequalities for the three-qubit Greenberger-Horne-Zeilinger and *W* states, Phys. Rev. A **65**, 032108 (2002).
[55] T. Zhong, J. M. Kindem, J. Rochman, and A. Faraon, Interfacing broadband photonic qubits to on-chip cavity-protected rare-earth ensembles, Nat. Commun. **8**, 14107 (2017).
[56] R. Holzinger, R. Gutiérrez-Jáuregui, T. Hönigl-Decrinis, G. Kirchmair, A. Asenjo-Garcia, and H. Ritsch, Control of localized single- and many-body dark states in waveguide QED, Phys. Rev. Lett. **129**, 253601 (2022).
[57] H. Ritsch, P. Domokos, F. Brennecke, and T. Esslinger, Cold atoms in cavity-generated dynamical optical potentials, Rev. Mod. Phys. **85**, 553 (2013).
[58] C. Luo, H. Zhang, V. P. W. Koh, J. D. Wilson, A. Chu, M. J. Holland, A. M. Rey, and J. K. Thompson, Cavity-mediated collective momentum-exchange interactions, arXiv:2304.01411.
[59] O. Hosten, R. Krishnakumar, N. J. Engelsen, and M. A. Kasevich, Quantum phase magnification, Science **352**, 1552 (2016).
[60] S. Welte, B. Hacker, S. Daiss, S. Ritter, and G. Rempe, Photon-mediated quantum gate between two neutral atoms in an optical cavity, Phys. Rev. X **8**, 011018 (2018).
[61] A. Periwal, E. S. Cooper, P. Kunkel, J. F. Wienand, E. J. Davis, and M. Schleier-Smith, Programmable interactions and emergent geometry in an array of atom clouds, Nature (London) **600**, 630 (2021).
[62] G. P. Greve, C. Luo, B. Wu, and J. K. Thompson, Entanglement-enhanced matter-wave interferometry in a high-finesse cavity, Nature (London) **610**, 472 (2022).
[63] Z. Li, S. Colombo, C. Shu, G. Velez, S. Pilatowsky-Cameo, R. Schmied, S. Choi, M. Lukin, E. Pedrozo-Peñafiel, and V. Vuletić, Improving metrology with quantum scrambling, Science **380**, 1381 (2023).
[64] P. Kirton, M. M. Roses, J. Keeling, and E. G. Dalla Torre, Introduction to the Dicke model: From equilibrium to nonequilibrium, and vice versa, Adv. Quantum Technol. **2**, 1800043 (2019).
[65] Z. Li, B. Braverman, S. Colombo, C. Shu, A. Kawasaki, A. F. Adiyatullin, E. Pedrozo-Peñafiel, E. Mendez, and V. Vuletić, Collective spin-light and light-mediated spin-spin interactions in an optical cavity, PRX Quantum **3**, 020308 (2022).
[66] V. Torggler, P. Aumann, H. Ritsch, and W. Lechner, A quantum N-queens solver, Quantum **3**, 149 (2019).
[67] J. Ramette, J. Sinclair, Z. Vendeiro, A. Rudelis, M. Cetina, and V. Vuletić, Any-to-any connected cavity-mediated architecture for quantum computing with trapped ions or rydberg arrays, PRX Quantum **3**, 010344 (2022).
[68] W. Huie, S. G. Menon, H. Bernien, and J. P. Covey, Multiplexed telecommunication-band quantum networking with atom arrays in optical cavities, Phys. Rev. Res. **3**, 043154 (2021).
[69] P. L. Ocola, I. Dimitrova, B. Grinkemeyer, E. Guardado-Sanchez, T. Dordevic, P. Samutpraphoot, V. Vuletic, and M. D. Lukin, Control and entanglement of individual Rydberg atoms near a nanoscale device, arXiv:2210.12879.